Proceedings of the ASME 2009 Conference on Smart Materials, Adaptive Structures and Intelligent Systems
SMASIS2009
September 21-23, 2009, Oxnard, California, USA

SMASIS2009-1359

DEVELOPMENT OF A SHAPE MEMORY ALLOY COMPOSITE ACTUATOR FOR THE WHOLE SKIN LOCOMOTION ROBOT

Eric Williams*
RoMeLa: Robotics and Mechanisms Laboratory
Department of Mechanical Engineering
Virginia Tech
Blacksburg, Virginia 24061
Email: ewilliams@vt.edu

Dennis Hong
RoMeLa: Robotics and Mechanisms Laboratory
Department of Mechanical Engineering
Virginia Tech
Blacksburg, Virginia 24061
Email: dhong@vt.edu

ABSTRACT

In this paper the development of a novel actuator is presented that utilizes a flexible shape memory alloy composite (SMAC) to generate motion for the Whole Skin Locomotion (WSL) robot. The WSL mechanism for mobile robots is inspired by how single celled organisms use cytoplasmic streaming to generate pseudopods for locomotion. This mobility mechanism is directly suited for robots traversing tight spaces where flexibility and shape changes are deemed necessary. The body of the WSL robot is comprised of an elongated fluid filled torus which turns itself inside out in a single continuous motion, effectively generating the overall motion of the cytoplasmic streaming ectoplasmic tube in amoebae. The eversion of the entire outer skin of the WSL is driven by a pair of the SMAC actuators in the shape of a torus. The actuation of the SMAC is accomplished by the individually controlled shape memory alloy wires embedded in an elastic beam that is then deformed into a torus shape. The design of the first prototype, fabrication efforts as well as a qualitative model of the behavior are presented. Experiments validating aspects of the modeling are also discussed.

NOMENCLATURE

R Bending radius of the SMAC actuator
r Cross sectional radius of the SMAC actuator
E_s Young's modulus of spring material
G_s Shear modulus of spring material
L Initial length of spring / SMA wire
D Outer diameter of spring
d Wire diameter of spring
J Polar moment of inertia of spring
n Number of coils in spring
T Tensile force in single SMA wire
A Cross sectional area of a single SMA wire
f Distributed force per unit arc length of actuator
τ Torque per unit arc length of actuator

INTRODUCTION

The WSL robot utilizes a novel locomotion strategy inspired by the cytoplasmic streaming of the amoeba [1]. The eversion of the WSL robot is the continuous translation from inside to outside and vice versa as pictured in Fig. 1. In order to generate the required motion, SMA wires are used to rotate a thin rubber tube which is connected end to end to then drive the outer skin of the elongated torus body. The motion of the SMAC actuator bent into a torus configuration is generated by an array of SMA wires embedded into silicone membrane which forms the inner torus and we will refer to this as the SMAC (Shape Memory Alloy Composite) actuator (Fig. 2,Fig. 3).

The WSL robot in its final form should be able to function autonomously in collapsed or constrained spaces. The nature of the motions of the WSL robot allow it to squeeze through

*Address all correspondence to this author.

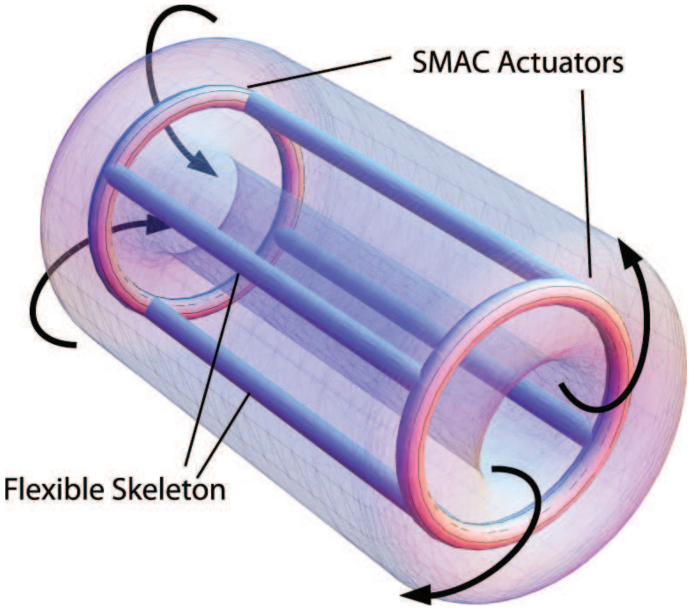

Figure 1. WSL robot with SMAC actuators as the driving mechanism

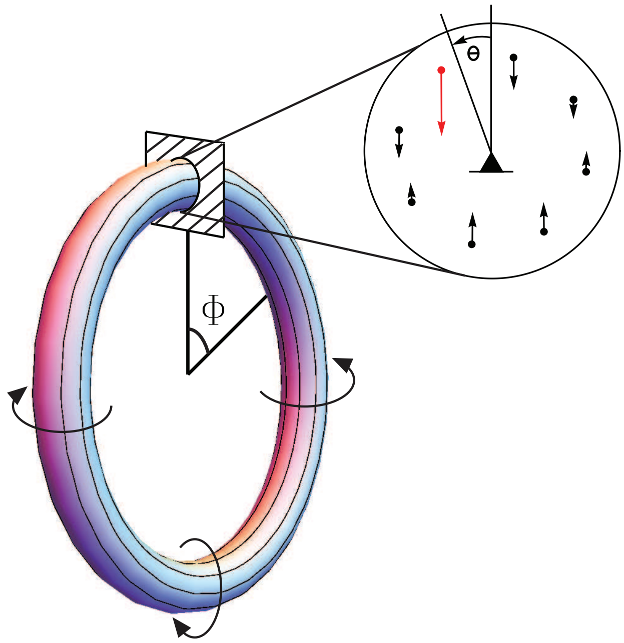

Figure 2. Diagram of the cross section for the actuator as a section view of the full torus. Also forces are shown from each wire with the currently heated wire in red.

tight spaces and possibly remains a candidate for traversing tight spaces in the human body for either endoscopic purposes or for drug delivery applications.

Continuum Robots

The realm of continuum robots is clearly one of the frontiers for robots of the future, where robots can use hierarchical compliance and flexibility to mimic and borrow the best aspects of nature's creatures [2]. The caterpillar robot proposed by Trimmer et al. uses SMA springs to grip while climbing obstacles [3]. Laschi et al. have developed a framework for a robotic octopus arm using electro-active polymers as artificial muscles that can bend and elongate their continuum actuator [4].

Continuum robots driven by SMA wires have been under investigation for medical applications [5]. The advances in colonoscopy and endoscopic robots have dramatically been influenced by continuum robots. Simaan et al have developed various tendon driven robots for minimally invasive surgery [6] [7].

A study of the motility mechanism of the WSL robot was performed by Hong et al [8]. A finite element study of the effect of contractile ring actuators on the exterior of the WSL robot demonstrated a potential candidate for propulsion force for the robot [8].

We are presenting a new approach to actuation in this paper that utilizes a torus that everts through itself using actuators embedded on the surface. Individual wires can be independently contracted by Joule heating such that the actuator rotates continuously (Fig. 1, Fig. 2).

Shape Memory Alloys

Shape Memory Alloys (SMA) are a group of metallic alloys that have micro-molecular properties that allow them to change shape drastically and recover large amounts of strain.

The crystalline structure of SMA allows it to transform from one solid phase to another solid phase and it is capable of reversible transformations [9]. The material is nonlinear elastic because of the multiple phases present yet the effective stiffness of the material can vary by a factor of 3 or more enabling force control. This change in stiffness gives SMAs the ability for applying a controlled force when embedded in a structure [10].

In order to utilize this material behavior to generate torque in an embedded actuator like the SMAC actuator, the calculation of stress in the material is necessary. This is typically done by the adaptation of previously derived constitutive models [10–12] or by deriving new constitutive relations analytically based on experimental results.

Since the control of these actuators should be able to handle the nonlinear behavior there has been extensive work on the control of these actuators. The nonlinear control of SMA wires has been investigated in detail by Elahinia et al. [13] and Grant [14].

The Young's Modulus for SMA depends on the ratio of the martensite phase and can be shown to be

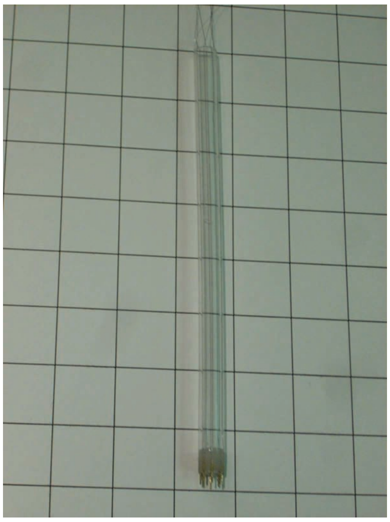

Figure 3. Picture displaying a portion of the SMAC actuator after mold removal

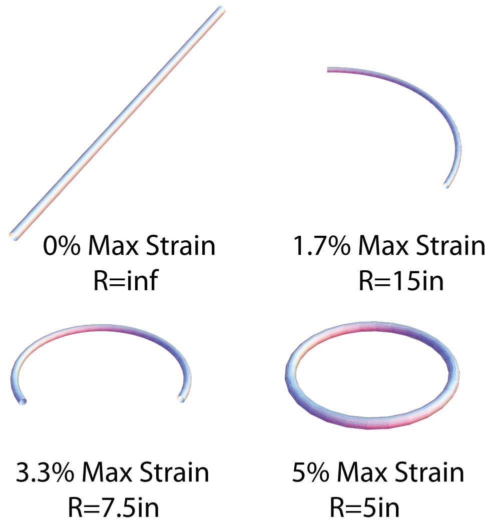

Figure 4. Bending of actuator into various radii of curvature and corresponding maximum bending strain values and radii of curvature values (L=400mm,r=6.35mm)

$$E_{SMA} = E_M + (E_A - E_M)(1 - \xi) \quad (1)$$

where E_M is the martensite Young's Modulus, E_A austenitic Young's Modulus and ξ is the martensite fraction.

SMA Composites

SMA materials offer relatively high strain when utilized as actuators or as passive elements. Lagoudas et al proposed a structure for the thermomechanical modeling of SMA composites [11]. More recently, Turner et al described the design and fabrication of a SMAHC (Shape memory alloy hybrid composite) [10]. The primary focus of the SMAHC was to make a hybrid composite involving an actuating material and a commonly used glass fiber composite. The temperature of the composite would not be controlled via external means, but would offer passive benefits to noise suppression using heat already present in the system. An application of the SMAHC material are described in further detail in Turner et al. [15].

Bruck et al. developed a SMA-polyurethane composite for two way bending. They adopted a method from the theory of flexible rods with the SMA wires modeled as a force and as a stiffness element [16]. The wires in their study were pre-strained such that selective heating could cause reversible bending [16].

The analysis of such structures typically involves a nonlinear finite element modeling approach using a ECTE (Effective Coefficient of Thermal Expansion) model [10]. This type of model allows commercial software packages to compute the thermomechanical response of SMA composites and particularly the SMAHC like the work of Turner et al [10] [15].

In this work, the authors have developed a shape memory alloy composite actuator using SMA wires and a silicone matrix. The actuator develops the eversion motion necessary for the WSL robot by principles described in the following section.

SMAC actuator

The Shape Memory Alloy Composite actuator, SMAC, starts as a straight beam with a circular cross section. The beam is bent into a torus introducing bending strains as can be seen in Fig. 4.

A number of wires are embedded along the length of the circular beam before the initial deformations are produced. Each of the wires are embedded with zero strain unlike the SMA composites previously mentioned [10, 11, 16]. The initial straining is performed after the matrix has set thus producing the actuation strains necessary to use the shape memory effect.

It was assumed that the classical Euler-Bernoulli beam theory with pure bending deformations was considered acceptable (equation 2). Assuming a linear deviation of stress and strain proportional to the distance from the neutral axis, the resultant moment can then be determined. This is an assumption that will require future inquiry, but will remain as a first cut in this preliminary work.

$$\frac{1}{R} = \frac{M}{EI} \quad (2)$$

The actuation of individual wires allows the recovery of bending strains in one portion of the cross section which effectively produces torque about the center of the cross section as pictured in Fig. 2. The net torque caused by the distributed force of the wires creates the everting motion. The distributed force from the wires, **f**, is depicted in Fig. 5.

MODELING OF THE SMAC

The behavior of the SMAC actuator is a multi-physics problem at its core. The actuation of the SMA wires in this actuator requires a temperature rise due to Joule heating and a decrease in temperature through conduction and convection. To generate the required torque the force in the actuator must be solved for from the equation of motion.

In order to generate the required motion from the actuator the proper selection of actuator material and structure was necessary. Since the strain in SMA wires is typically limited to 5% for moderate cycle applications, the actuator design should should have this as a major criterion [17].

The initial strain in the actuator is assumed to be from pure bending, so the strain exhibited in the wires depends on the distance from the neutral axis and the curvature. The strain of the wires at the neutral axis, **R**, is zero so that is the reference length. The distance from the neutral axis changes as the wires rotate around the center of the actuator's cross section.

It is assumed that the actuator be rigid in the **r** direction, so the displacement in each wire is only a function of θ. It is also assumed that the displacement of each wire varies as it rotates around the cross section such that

$$\triangle L = 2\pi r \cos(\theta) \tag{3}$$

The engineering strain of the SMA wire i is defined as the change in length over the initial length

$$\varepsilon(\theta_i) = \frac{\triangle L}{2\pi R} = \frac{r}{R}\cos(\theta_i) \tag{4}$$

where **r** is the radius of the actuator cross section and **R** is the radius of curvature of the actuator [18].

The torque available in the actuator is determined by the change in the stiffness and the displacement of each wire as the SMA material is transformed from the soft phase of martensite to the stiff phase of austenite. Stiffness of the wires can be determined and this can be used to determine what force output is possible. For the geometry of the SMAC, a transformation is required to determine the distributed radial force **f** generated in each wire with a given tensile force, **T** (Fig. 5) [1]. It is assumed that the wires do not buckle in compression as they are supported by the matrix so that the stiffness in compression does not require a post buckling analysis. The stiffness in compression is assumed to be the same as the stiffness in tension.

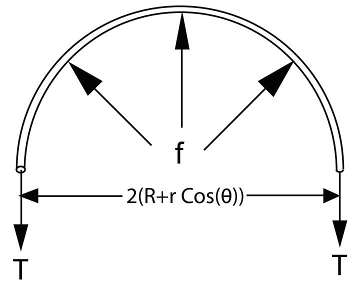

Figure 5. Diagram of tensile force to distributed radial force for one wire

$$f = \frac{T}{R} \tag{5}$$

The torque exerted on the actuator by the wires can be determined from the sum of the torque in each wire as depicted in Fig. 6. Since this torque is about the center of the cross section (Fig. 2) and is a sum of a distributed forces at a distance, **r**, from the center of rotation the units are in Newtons. To determine the torque of the actuator an integration of these distributed torques along the ϕ-direction is necessary (Fig. 2).

$$\tau_{wire} = \frac{Tr\sin(\theta)}{R + r\cos(\theta)} \tag{6}$$

The stiffness in the wires is defined the same as the stiffness of a rod.

$$k_{sma} = \frac{AE_1}{2\pi R} \tag{7}$$

The torque generated from one wire when $T = k_{SMA} r \sin(\theta)$ becomes

$$\tau_{wire} = \frac{k_{sma} r^2}{R + r\cos(\theta)} \cos(\theta)\sin(\theta) \tag{8}$$

and using trig identities simplifies to

$$\tau_{wire} = \frac{k_{sma} r^2 \sin(2\theta)}{2(R + r\cos(\theta))}. \tag{9}$$

The maximum torque output from the actuator is determined by a sum of the individual wire torques shown in equation 9.

Table 1. Stiffness of martensite phase ($\frac{N}{mm}$) and austenite phase for select Dynalloy Flexinol^{TM} wires with a 2πR unstretched length

Wire Diameter	k_A	k_M
$50\mu m$	0.185	.0689
$75\mu m$	0.415	0.155
$100\mu m$	0.738	0.276
$150\mu m$	1.661	0.620
$200\mu m$	2.953	1.102

The actuation of one quadrant of wires produces a torque that is proportional to the number of wires and the difference in their torques with another unactuated quadrant.

The maximum torque in the actuator occurs when one quadrant of wires is fully heated and the other three are cool. During operation this state will not be maintained as the wires have a finite cooling time which is based on the heat transfer. And it may come from intuition that when all wires are at the same temperature and phase the torque is zero. Since the maximum torque available from the actuator has been described it is possible to determine the maximum torque once depending on the number of SMA wires.

For the case of 8 wires, the maximum torque that can be generated is when one wire is actuated. The maximum torque for this situation is the difference in torques of two wires having a martensite fraction, ξ, of 0 and 1 while being separated by $\frac{\pi}{2}$ radians. The equation for the maximum torque in this case is

$$\tau_{max-pair} = \frac{r^2}{2(R+r)}(k_A - k_M) \tag{10}$$

where the austenite stiffness is k_A and the martensite stiffness is k_M. The stiffness of the wire in the martensite form is softer than the austenite form and a table of Dynalloy Flexinol^{TM} is shown in table 1.

Composite Model

The composite properties can be modeled using a representative volume element in a finite element package or the Rule of Mixtures (ROM) directly [19]. For this study, the ROM was selected to determine the effective properties of the actuator.

Using the ROM the flexural stiffness for the actuator can be determined. The ROM approach "smears" the properties of the SMA wire and the rubber matrix material together to get an approximate Young's Modulus, $\mathbf{E_1}$, and other properties. [19]. The volume fraction of the wires in the matrix, $\mathbf{V_{SMA}}$, determines to what level the wire's properties play in the role of the composite.

In order to get the properties of the rubber material, tensile tests were performed through the operating strain range of the material. The properties agreed well with a linear elastic model with a Young's Modulus of 1MPa and the material was assumed to be incompressible. The properties of the SMA wire are taken from the datasheet provided by Dynalloy.

Since the first representation of the bending is a 1D case, only the effective Young's modulus, E_1, is needed. It can be shown from Hyer et al [19]

$$E_1 = E_f V_f + E_m V_m \tag{11}$$

where E_f is the Young's modulus of the fibers, E_m is the Young's modulus of the matrix and V_f and V_m correspond to the volume fraction of the fibers and matrix respectively.

Since pure bending is introduced into the beam for the initial displacements of the wires, the flexural rigidity is defined as the moment required to bend the composite beam a unit curvature.

$$\beta_{SMAC} = E_1 I \tag{12}$$

The area moment of inertia for the beam is that of a hollow circular section.

$$I = \frac{\pi}{64}(D^4 - d^4) \tag{13}$$

For the case of the actuator we should sum the flexural rigidities of the spring and the composite.

$$\beta = \beta_{spring} + \beta_{SMAC} \tag{14}$$

Dynamic Model

The actuator generates an everting motion from the supply of voltage to the wires, so a torque balance about the center of the cross section was performed (Fig. 2). Since there are no rigid supports attached to the actuator in this simplified model there is no stiffness term, however it is assumed that there is a small viscous drag that restricts the motion.

$$\sum \tau_{external} + \sum_{i=1}^{n} \tau_{wires} + c\dot{\theta} = J\ddot{\theta} \tag{15}$$

The torque generated by the actuator is dependent on the sum of the torque from the distributed forces in the wires. When the temperature in the wires rises above the phase transformation temperature the wires contract thus generating stress and creating the distributed force as in Fig. 5. This distributed force creates torque which produces the desired motion.

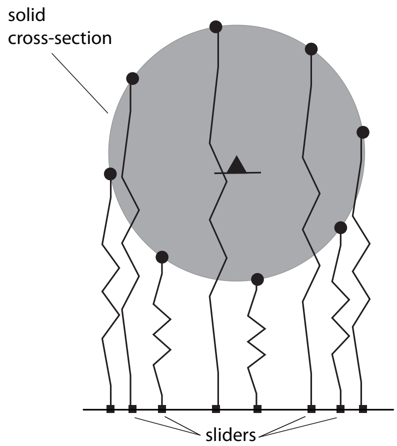

Figure 6. Single state reduced model

Heat Transfer Model

Since the temperature of the SMA wires is a crucial part of the actuation, the heat transfer modeling of the actuator is very important to the design process. The rubber material considered for this prototype is a silicone elastomer with insulating properties, so the exchange of heat into the environment involves the conduction of heat through the silicone then convection on surface of the actuator. The actuator is fluid filled allowing for better heat exchange from the SMA wires.

The heat transfer is a 3D problem like that of the deformations yet simplifications were made to make the problem tractable. It was assumed that the heat transfer occurs only in the plane of the cross section reducing the problem to a 2D transient diffusion problem cast in polar coordinates (r, ϕ).

$$C\rho\frac{\partial\theta}{\partial t} = \frac{k}{r}\frac{\partial}{\partial r}\left(r\frac{\partial\theta}{\partial r}\right) + \frac{k}{r^2}\left(\frac{\partial^2\theta}{\partial\phi^2}\right) \tag{16}$$

Since the transformation of the SMA wires is performed by Joule heating, the energy generation in the SMA wires is proportional to I^2R. In order to get a continuous everting motion from the actuator, the wires are heated in one portion of one quadrant of the cross section, thus the heating is dependent on the motion of the actuator. To simulate the heat transfer portion of the model without the full thermomechanical behavior present, it is necessary to estimate the rotation period and attempt to heat the wires at the same frequency with their prospective phase.

Bending of Actuator

In order to determine the overall flexural rigidity of the actuator consisting of the matrix material, wires and helical spring core it is necessary to determine their individual components of rigidity. The actuator is configured such that there is an initial radius of curvature in which the wires are strained allowing the everting motion.

The matrix material selected was Sylgard 184^{TM} from Dow Corning. Syglard 184^{TM} has optical clarity and high strain capacity ($> 140\%$). Tensile tests were performed on tube samples that are equivalent in size to the SMAC matrix without the SMA wires. The Young's modulus was determined from these tests(1MPa). Since the material will only exhibit strains in the ($\varepsilon < 5\%$) strain range, the correlation of test data with this linear fit was high ($> 0.998\%$). As with most rubbers, the material is considered incompressible ($\nu = 0.5$).

The bending of tubes of this geometry comprised of Sylgard 184^{TM} showed Brazier type flattening and collapse at relatively low curvatures [20]. To reduce weight, increase flexibility and allow for better heat convection for the wires it was determined to make the actuator hollow. An open helical spring was found to be a sufficiently rigid way of preventing that types of collapse and it would help to stiffen the actuator in the **r**-direction. Therefore, the deformations for this study assume that an open helical spring restricts the tube from this type of collapse.

For the modeling of the bending for the open helical spring, several analytical models are available [21]. For a general helical spring with a low helix angle ($< 30^o$) the Timoshenko model has been shown to be accurate experimentally and was selected for this work [21].

The flexural rigidity, β_{spring}, is defined as the ratio of bending moment, M, to the curvature, R.

$$\beta_{spring} = \frac{M}{1/R} = \frac{4LE_sJG_s}{n\pi(D-d)(2G_s+E_s)} \tag{17}$$

The flexural rigidity for the spring in our prototype was determined to be approximately 117.5 N-mm^2 using equation 17. The moment required to bend the spring into the configuration for the prototype was approximately 0.92 N-mm as our radius of curvature, **R**, is equal to 127mm.

As shown in equation 2, the flexural rigidity for the composite part of the actuator is determined by the volume fractions of fibers and matrix material.

To design the actuator for flexural rigidity and actuating torque the effective Young's modulus for the material is the first parameter to be considered. Using the ROM approach from

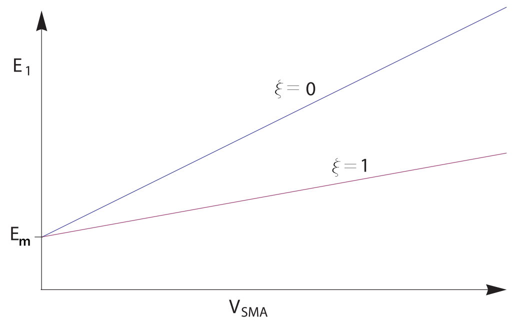

Figure 7. Design curves for Young's modulus considering SMA wire volume fraction and martensite fraction

equation 11 combined with the effect of martensite fraction on $\mathbf{E_{SMA}}$ as in equation 18 one can determine the effective Young's modulus in the axial direction, $\mathbf{E_1}$, with the relation shown in equation 18.

$$E_1 = (E_M + (E_A - E_M)(1-\xi))V_f + E_m(1-V_f) \qquad (18)$$

ACTUATOR DESIGN AND CONSTRUCTION

To reduce weight and allow for better heat convection for the wires it was determined to make the actuator hollow. However, this caused the Brazier type buckling would to be a potential failure mode. It was determined that utilizing a helical spring inside the actuators would support the tubes from bending collapse and add rigidity to the structure. The springs were chosen to be soft enough to bend easily but provide the required rigidity to support the tubes against collapsing. For a collapsed structure environment, the flexural stiffness of the actuator becomes very important to the stability and operability.

One of the main challenges of this work was to fabricate the prototype used in this study. Fixturing SMA wires seems to be the greatest difficulty prior to and during casting. The procedure for casting will be outlined in a future paper.

Prior to embedding, the wires are loaded and actuated repeatedly for 100 cycles in an attempt to reduce creep following the technique of Barnes et al [15]. In order to return the wires to their unstrained state they are individually heated with an industrial heat gun.

For flexibility and tear strength a rubber compound was selected that would be light and able to be cast around the SMA wires to fabricate the actuator. Liquid rubber mixtures are commercially available and are relatively easy to mold. The challenge with manufacturing composites with rubber materials is typically the viscosity of the rubber and the problem of air bubbles in the mold. Vacuum degassing was used to remove many of

Figure 8. Prototype in experimental jig

the bubbles and the added benefit of transparency of the Sylgard 184 allowed for the supervision of wire alignment and the bubble removal.

For this preliminary proof of concept, the number of wires was selected such that the flexural stiffness was a moderate value and the torque in the actuator would be measurable. For the prototype used in this study, 8 wires were used each with a $150\mu m$ diameter.

The wires and electrical parts were also cast in urethane plastic in order to construct the electrical connections to the slip ring used for connecting the actuator segment to the power supply.

The actuator segment fabricated for this study was a 1/4 torus and is pictured in its original unbent form in Fig. 8. The experimental jig used to hold the actuator in the 90 degree arc was laser cut and the bearing holders were fabricated using a CNC machine.

CONCLUSIONS AND FUTURE WORK

From the initial proof of concept experiments much was learned about the qualitative behavior of the SMAC actuator. The first prototype exhibited the ability to rotate when set into the experimental jig, but due to manufacturing issues the actuator showed signs of damage that caused dislocations of the wire from the matrix. It could be seen that the compression of the wires on the inside of the SMAC causes them to buckle, this has a softening effect on the stiffness of the wires as they are in compression. It was also assumed that the SMAC actuator did not have any axial deformation as it was bent, however this assumption was found to be incorrect with the current prototype and a re-evaluation of equation 2 is now underway.

However, the initial prototype did not fail before we could learn from it. The assumption of a uniform torque generated by the actuator spread over the entire perimeter was not entirely valid for a quarter section of the SMAC actuator. Also the pure bending assumptions did not capture the complete behavior of the actuator as could be seen from the preliminary experiments.

Further refinements to the model will be expanded upon in future works on the actuator, such as the coupled thermo-mechanical FEA approach for the actuation. The full 3-dimensional model will likely provide more insight to the behavior and ways to make the actuation more optimal.

The properties of the wire used in this study were provided by the supplier, but plans for future testing of the wire have been made to check the presented property values. Digital image correlation (DIC) methods will be employed in future tests to map the deformation behavior of the SMAC actuator to check assumptions more closely.

It was determined that modeling the dynamic behavior of the SMAC actuators should be conducted with a nonlinear FE analysis allowing full 3D strains similar to the work of Turner et al. [15]. Also the implementation of a constitutive model such as the one derived by Lagoudas et al. or the modified version of the work by Bruck et al. [11] [16].

Since the focus of this work was the preliminary proof of concept, open loop control methods were employed, however a closed loop controller for the actuator is under investigation.

ACKNOWLEDGMENT

The authors would like to thank the National Science Foundation for their support for this work under Grant No. CMMI-0643839. Also the authors would like to thank our NSF REU Taylor Young and Allison McCormack who worked as undergrad researchers aiding in the construction process of the SMAC.

REFERENCES

[1] Ingramm, M., 2006. "Whole skin locomotion inspired by amoeboid, motility mechanisms: Mechanics of the concentric solid tube model". *MS Thesis, Virginia Polytechnic Institute and State University*, August.

[2] Bailey, S. A., Cham, J. G., Cutkosky, M. R., and Full, R. J., 2001. "Comparing the locomotion dynamics of the cockroach and a shape deposition manufactured biomimetic hexapod". *Lecture Notes in Control and Information Sciences, Experimental Robotics VII,* ***271***, pp. 239–248.

[3] Trimmer, B. A., Takesian, A. E., Sweet, B. M., Rogers, C. B., Hake, D. C., and Rogers, D. J., 2006. "Caterpillar locomotion: A new model for soft-bodied climbing and burrowing robots". *7th International Symposium on Technology and the Mine Problem, Monterey, CA*, May.

[4] Laschi, C., Mazzolai, B., Mattoli, V., Cianchetti, M., and Dario, P., 2009. "Design of a biomimetic robotic octopus arm". *Bioinspiration and Biomimetics,* ***4***(015006), March, pp. 1–8.

[5] Ikuta, K., Tsukamoto, M., and Hirose, S., 1998. "Shape memory alloy servo actuator system with electric resistance feedback and application for active endoscope". *IEEE International Conference on Robotics and Automation, Philadelphia, PA, USA*, April.

[6] Simaan, N., Taylor, R. H., and Flint, P., 2004. "A dexterous system for laryngeal surgery: Multi-backbone bending snake-like slaves for teleoperated dextrous surgical tool manipulation". *IEEE International Conference on Robotics and Automation*, pp. 351–357.

[7] Xu, K., and Simaan, N., 2008. "An investigation of the intrinsic force sensing capabilities of continuum robots". *IEEE Transactions on Robotics,* ***24***(3), June, pp. 576–599.

[8] Hong, D., Ingram, M., and Lahr, D., 2009. "Whole skin locomotion inspired by amoeboid motility mechanisms". *ASME Journal of Mechanisms and Robotics,* ***1***(1), February, pp. 0110151–0110157.

[9] Brinson, L., 1993. "One-dimensional constitutive behavior of shape memory alloys: Thermomechanical derivation with non-constant material functions and redefined martensite internal variable". *Journal of Intelligent Material Systems and Structures,* ***4***(2), pp. 229–242.

[10] Turner, T. L., 2001. "Thermomechanical response of shape memory alloy hybrid composites". *NASA Technical Memorandum-2001-210656*, pp. 16–23.

[11] Boyd, J. G., and Dmitris C. Lagoudas, D., 1994. "Thermomechanical response of shape memory composites". *Journal of Intelligent Material Systems and Structures,* ***5***(3), pp. 333–346.

[12] Daghia, F., Inman, D., Ubertini, F., and Viola, E., 2008. "Shape memory alloys hybrid composites for shape and stiffness control". *Journal of Intelligent Material Systems and Structures,* ***19***(5), pp. 609–619.

[13] Elahinia, M. H., and Ashrafiuon, H., 2002. "Nonlinear Control of a Shape Memory Alloy Actuated Manipulator". *Journal of Vibration and Acoustics,* ***124***, October, pp. 566–575.

[14] "Grant, D.".

[15] TURNER, T. L., BUEHRLE, R. D., CANO, R. J., and FLEMING, G. A., 2004. "Modeling, fabrication, and testing of a sma hybrid composite jet engine chevron concept". *Journal of Intelligent Material Systems and Structures,* ***17***(6), pp. 483–497.

[16] Bruck1, H. A., Moore, C. L., and Valentine, T. L., 2002. "Repeatable bending actuation in polyurethanes using opposing embedded one-way shape memory alloy wires exhibiting large deformation recovery". *SMART MATERIALS AND STRUCTURES,* ***11***, pp. 509–518.

[17] "Muscle wires project book". p. 5.
[18] Shigley, J. E., Mischke, C. R., and Budynas, R. G., 2003. *Mechanical Engineering Design*. McGraw Hill.
[19] Hyer, M., 2009. *Stress analysis of fiber-reinforced composite materials*. DEStech Publications.
[20] Fabian, O., 1981. "Elastic-plastic collapse of long tubes under combined bending and pressure loads". *Ocean Engineering,* ***8***(3), pp. 295–330.
[21] Reggiani, B., 2007. "Simulation models in biomechanics and experimental mechanics". *Ph.D. Thesis, Dipartimento di Ingegneria delle Costruzioni Meccaniche, Nucleari, Aeronautiche e di Metallurgia, Universit degli Studi di Bologna*.